PAPER

Check for updates

Solution processed double-decked V$_2$O$_x$/PEDOT:PSS film serves as the hole transport layer of an inverted planar perovskite solar cell with high performance†

Zhiyong Liu, [iD] *[ab] Tingwei He,[ab] Kaikai Liu,[a] Qinqin Zhi[a] and Mingjian Yuan*[abc]

In this paper, we have reported a high-performance inverted planar perovskite solar cell (PSC) with double-decked hole transport layer (HTL) sandwiched between the indium tin oxide (ITO) electrode and the perovskite photoactive layer. The double-decked HTL film is fabricated by coating inorganic vanadium oxide (V$_2$O$_x$) layer and poly(3,4-ethylene dioxy-thiophene)–poly(styrene sulfonate) (PEDOT:PSS) layer. In this study, double-decked V$_2$O$_x$/PEDOT:PSS HTL film can improve the optoelectronic properties of PSC device. It has been found that the double-decked V$_2$O$_x$/PEDOT:PSS film plays a crucial role in enhancing charge transfer rate and suppressing electron–hole pair recombination. The valence of vanadium in the V$_2$O$_x$ has been changed by adjusting the molar ratio of V$_2$O$_5$ to H$_2$O$_2$. The PSC can reach its best performance when V$_2$O$_5$ and H$_2$O$_2$ react at a molar ratio of 1 : 60. In addition, the concentration of the V$_2$O$_x$ aqueous solution has also been changed to optimize performance of PSC. Hence, the device with double-decked V$_2$O$_x$/PEDOT:PSS HTL film can increase the power conversion efficiency (PCE) to 15.86%, higher than that of reference device with PEDOT:PSS (13.56%). Besides, compared with reference device, our device has a better repeatability in the preparation process.

1. Introduction

Due to its excellent photo-electronic properties including low exciton binding energy ($\sim$30 meV),[1] high extinction coefficient ($\sim$10^4–10^5 cm^{-1}),[2,3] and long carrier diffusion lengths in thin films (>1 μm),[4,5] the organic inorganic halide perovskite-based solar cell (PSC) have attracted considerable attention in the field of solar cells and made remarkable progress in recent years.[6–9] Since 2009, the power conversion efficiency (PCE) of PSC has been increased from 3.8% to 22.1%,[10,11] which is unexpected and unprecedented in the field of organic photovoltaics. The PSC can be divided into two types: one with scaffold metal oxide layer and the other without the scafford metal oxide layer like perovskite active layer sandwiched between the hole transport layer (HTL) and electron transport layer (ETL).[12–15] The scaffold metal oxide layers have to be prepared under high-temperature conditions, such as Al$_2$O$_3$ or TiO$_2$ on indium tin oxide (ITO) or fluorine doped tin oxide (FTO).[16] The planar heterojunction (PHJ) PSC without the scafford metal

oxide layer can also be classified into two categories: regular configuration (n–i–p, ETL/CH$_3$NH$_3$PbI$_{3-x}$Cl$_x$/HTL),[17] and inverted configuration (p–i–n, HTL/CH$_3$NH$_3$PbI$_{3-x}$Cl$_x$/ETL).[18] Owing to its low-temperature fabrication method, excellent performance and sharply-reduced hysteresis,[19] PSC with inverted p–i–n structure will have a promising prospect in the future.

The poly(3,4-ethylene dioxy-thiophene)–poly(styrene sulfonate) (PEDOT:PSS) is usually used as HTL to enhance crystallinity of the perovskite layer film.[20–22] We find it easy to collect the holes *via* the PEDOT:PSS layer, because PEDOT:PSS has many advantages over others such as good conductivity, smooth morphology, high work function (WF) and high transparency.[23] The PCE of the inverted planar PSCs has been improved significantly by PEDOT:PSS HTL film. What merits much attention is that lots of research works have been carried out to enhance performances of PSCs, except PEDOT:PSS HTL film.[24,25] Some researches have been conducted to use inorganic transition metal oxides including nickel oxide (NiO$_x$),[26–29] lead sulfide (PbS),[30] and molybdenum oxide (MoO$_x$)[31–33] as the HTL film. The conduction levels of the oxides are much higher than the lowest occupied molecular orbital (LOMO) of the organic layers, which can prevent electrons from transporting in the wrong directions and improve the photo current of PSCs. However, most transition metal oxides films are thermally evaporated onto the substrates in vacuum and will hardly be applied to commercial production process of PSC devices due to its high cost.[34,35]

^{a}Department of Physics and Materials Science, Henan Normal University, Xinxiang 453007, China. E-mail: zyliu01@163.com

^{b}Henan Key Laboratory of Photovoltaic Materials, Xinxiang 453007, China

^{c}Department of Chemistry, Nankai University, Tianjin 300071, China. E-mail: yuanmj@nankai.edu.cn

† Electronic supplementary information (ESI) available. See DOI: 10.1039/c7ra04414c

Recently, some techniques based on a lower-cost, simpler and more controllable approach have been reported.[36] Some solution-processed bilayer HTLs have been used in solar cells, such as graphene oxide (GO)/PEDOT:PSS,[37] MoO_3/PEDOT:PSS,[38] and PEDOT:PSS/vanadium oxide (V_2O_x).[39] Whereas, these cells do not show a higher PCE. Here we use double-decked V_2O_x/PEDOT:PSS as HTL of PSCs, by contrast, the higher efficiency and better repeatability of the devices has been achieved by changing the valence of vanadium of double-decked V_2O_x/PEDOT:PSS film.

The vanadium pentoxide (V_2O_5) and its derivative compounds have been researched intensively due to their redox activity.[40–42] The V_2O_x can be obtained by a simple method of synthesis that uses V_2O_5 and hydrogen peroxide (H_2O_2) as starting material at a low temperature. Through this method, the vanadium element produces a variety of binary compounds with the chemical general formula VO_{2+x} ($-0.5 \leq x \leq 0.5$), such as V_2O_3, VO_2, V_2O_5, V_3O_7, V_4O_9, V_6O_{13}.[43] The V_2O_x with different valences can be prepared by controlling the molar ratio of V_2O_5 to H_2O_2. In this work, the double-decked V_2O_x/PEDOT:PSS films prepared by spin-coating V_2O_x and PEDOT:PSS solution can serve as the HTL to enhance charge transfer rate and suppress electron–hole pair recombination in PSCs. Here we report a high-performance inverted planar PSC device with the structure of ITO/V_2O_x/PEDOT:PSS/$CH_3NH_3PbI_{3-x}Cl_x$/the phenyl-C_{61}-butyric acid methyl ester (PCBM)/Ag. The maximum PCE of 15.86% has been achieved by controlling the optimum concentration of the V_2O_x solution. An average power conversion efficiency (PCE_{AVE}) of has been increased significantly from 11.85% (the PCE_{AVE} of 30 reference devices with PEDOT:PSS HTL) to 14.97% (the PCE_{AVE} of 120 controllable devices with the double-decked V_2O_x/PEDOT:PSS HTL).

2. Experimental

2.1 Materials and preparation

Chlorobenzene (C_6H_5Cl), hydrogen iodide (HI), methylamine (CH_3NH_2), hydrogen peroxide (H_2O_2, 30%) and V_2O_5 powder were purchased from Shanghai Chemical Industry Co. The PEDOT:PSS was bought from Heraeus (Germany). $PbCl_2$ (99.999%) and N,N-dimethylformamide (DMF) (anhydrous, amine free; 99.9%) were purchased from Alfa-Aesar. The $PC_{61}BM$ was produced by Nichem Fine Technology Co., Ltd. (Taiwan). CH_3NH_3I was synthesized by CH_3NH_2 and HI according to the reported procedure.[44] $CH_3NH_3PbI_{3-x}Cl_x$ solutions were fabricated by solubilizing CH_3NH_3I and $PbCl_2$ in DMF with a molar ratio of 3 : 1, and agitating the compound in a glove box filled with N_2 at 60 °C for 12 h. PCBM solutions were manufactured by dissolving PCBM powder in chlorobenzene and churning the mixture in a N_2 glove box for 12 h, with an optimized concentration of 20 mg mL^{-1}.

2.2 Fabrication of the double-decked V_2O_x/PEDOT:PSS film

First, V_2O_5 aqueous solution was manufactured by dissolving 15 mg of V_2O_5 powder in 5 mL of deionized water and churning the mixture in air at room temperature for 30 min, with

a concentration of 3 mg mL^{-1}. Second, the 0.6 mL of H_2O_2 aqueous solutions (30%) was added to V_2O_5 aqueous solution, the mixture was stirred for 10 min and let set for 10 h or more. As a result, the V_2O_x aqueous solution was prepared. V_2O_x aqueous solution prepared was filtered through a 0.22 μm pore-size filter membrane, spin-coated at 5000 rpm for 40 s on clean ITO substrates and dried at 150 °C for 10 min. Then, PEDOT:PSS solution filtered was spin-coated at 4500 rpm for 40 s on V_2O_x films and dried at 140 °C for 20 min. Through this procedure, we have prepared a double-decked V_2O_x/PEDOT:PSS thin film with a thickness of about 40 nm.

2.3 Fabrication of the PSC device

13 × 15 mm ITO glass (Fine Chemicals Industry Co., Gyeonggi-do, Korea, 10 U sq^{-1}) was patterned by the method mentioned.[45] And the substrate etched was brushed by a cotton ball with detergent repeatedly. Then, in order to remove water-soluble and organic impurities on the substrate, we must clean ITO coated glass in deionized water, ethanol and acetone twice respectively, with ultrasound for 15 min or more. After being washed, the substrate was dried in the dry box at 60 °C for 30 min and treated in UV-ozone cleaner for 10 min. Then the double-decked V_2O_x/PEDOT:PSS thin film was prepared on clean ITO coated glass through the method described above. To prepare the perovskite layer film, the $CH_3NH_3PbI_{3-x}Cl_x$ solution was spin-coated onto the double-decked V_2O_x/PEDOT:PSS film layer at 4000 rpm for 40 s in a N_2 glove box. The annealing of wet perovskite films was carried out by adopting a typical gradient increased temperature method that can be seen elsewhere.[46–48] The substrates were slowly heated from 30 to 60 °C at a ramp rate of 10 °C/5 min and from 60 to 100 °C at a ramp rate of 10 °C/10 min on a hot plate, and the perovskite layer films were dried at 100 °C for 90 min. After that, PCBM film was deposited by spin-coating at 2000 rpm for 40 s onto perovskite layer film in a N_2 glove box. Finally, the substrates were transferred to a vacuum chamber for silver electrode evaporation. The silver film was thermally deposited onto the PCBM film under vacuum at 4.5×10^{-5} Pa through a shadow mask, defining single device area of 6.25 mm^2.

2.4 Characterizations

The surface and section morphology were characterized by a field emission scanning electron microscope (FESEM, Quanta 200 FEG, FEI Co.). The Energy dispersive spectroscopy (EDS) was carried out by an EDS device connected to FESEM. The atomic force microscope (AFM) images were collected by an Agilent 5500 SPM system (Agilent Technologies, USA). The crystalline phase and X-ray diffraction (XRD) patterns of perovskite films were recorded on a Rigaku D/MAX-2400 diffractometer. X-ray photoelectron spectroscopy (XPS) measurements were performed by using an AXIS Ultra instrument (Kratos UK) at a base pressure of $\sim 10^{-8}$ Torr and 295 K. The WF of V_2O_x films were measured through UPS (Riken Keiki). Steady-state photoluminescence (PL) measurements were conducted by using an Edinburgh FLS980 fluorescence spectrophotometer with an excitation at 470 nm. The current density–voltage (J–V) curves were measured (2400 Series Source

Meter, Keithley Instruments) under simulated Air-Mass (AM) 1.5 sunlight at 100 mW cm^{-2} (Newport, Class AAA solar simulator, 94023A-U). The incident-photon-to-current efficiency (IPCE) measurement was performed through a system combining a xenon lamp, a monochromator, a chopper and a lock-in amplifier together with a calibrated silicon photodetector. UV-Vis absorption measurements were carried out by using Shimadzu UV-2550 spectrometer. The electrochemical impedance spectroscopy (EIS) measurements were conducted on a CHI660C electrochemical work station (Shanghai, China) with 5 mV alternating current (AC) amplitude at a frequency range of 10^6 Hz to 1 Hz.

## 3.   Results and discussion

3.1   Double-decked V_2O_x/PEDOT:PSS HTL film

In our study, V_2O_x aqueous solution is prepared by the chemical reaction between V_2O_5 and H_2O_2, as mentioned in the Experimental section. Probably, a process of the chemical reaction can be interpreted as follows: V_2O_5 powder is dissolved partially in deionized water at the beginning of chemical reaction process; the metal cations (V^{5+}) are generated by molecules of water. The reaction mentioned above is (eqn (1)).

$$V_2O_5 + H_2O \rightarrow V_2O_5 \cdot nH_2O \tag{1}$$
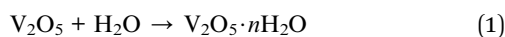
The reaction has increased acidity of the solution.[49] The $V_2O_5 \cdot nH_2O$ molecule is dissociated by adding H_2O_2, forming the peroxovanadate. Therefore, the degree of acid hydrolysis is controlled by acidic precursor phase solution (eqn (2)).[50]

$$V_2O_5 \cdot nH_2O + H_2O_2 \rightarrow H_3VO_4 \tag{2}$$
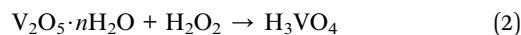
The peroxovanadate is not very stable in aqueous solution. The partial stability of peroxovanadate in metastable phase is achieved when aqueous solution is let set for 10 h or more (partially oxidation of V^{5+} to V^{4+} ions), resulting in the formation a mixture of vanadium oxide (eqn (3)).

$$H_3VO_4 \rightarrow V_2O_x \cdot nH_2O \tag{3}$$
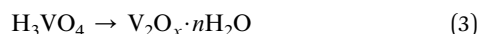
XPS was used to investigate composition of the V_2O_x thin film with the optimal molar ratio of V_2O_5 to H_2O_2. High resolution XPS spectrum corresponding to V is shown in Fig. 1a. As shown in the images, the V 2p spectrum can be well fitted with $2p_{1/2}$ and $2p_{3/2}$ doublets by a Gaussian function, which corresponds to vanadium in two different oxidation states (V^{5+} and V^{4+}). Two peaks at the binding energy (BE) of 517.7 and 525.1 eV are corresponding to the 2p doublet of V^{5+}. And the other two peaks at the BE of 516.7 and 524.1 eV are correspond to the 2p doublet of V^{4+} respectively. The atomic concentration ratio of V^{5+} to V^{4+} is about 1.41 : 1 according to the area ratio of their peaks, implying that ~41.5% V^{4+} exists in the V_2O_x film layer. The V^{4+} ions in V_2O_x film could result in the enhancement of conductivity of the HTL,[51] which facilitates the transport and collection of charge carrier in the PSC. EDS can qualitatively and quantitatively analyze all elements of the sample. The V_2O_x solution is spin-coated on the polished monocrystalline silicon wafer rather than the ITO coated glass. The reason is that wafers have a lower roughness compared with the ITO film surface, which helps observe clearly the cross-section image of V_2O_x film. As shown in Fig. 1b–d, the cross-section FESEM image together with vanadium elemental mapping and EDS spectrum are performed on V_2O_x film based on monocrystalline silicon. The signals of V content of V_2O_x film material were clearly observed. Moreover, it is important for us to point out that peaks of $2p_{1/2}$ and $2p_{3/2}$ coral electron are also clearly identified at 524.9 and 517.5 eV respectively in the XPS spectrum of the V_2O_x film.

Fig. 2a and b show the schematic illustration and associated cross-section FESEM image of the prepared inverted PHJ PSC device with the structure of ITO/V_2O_x/PEDOT:PSS/CH_3NH_3-$PbI_{3-x}Cl_x$/PCBM/Ag. The double-decked V_2O_x/PEDOT:PSS thin film (~40 nm) is used as the HTL on the ITO bottom electrode (~200 nm) of PSC device. $CH_3NH_3PbI_{3-x}Cl_x$ film (~250 nm) is chosen as photoactive layer, PCBM film (~45 nm) as ETL and Ag film (~150 nm) as top electrode. The energy level diagram corresponding to each layer of the PSC has been shown in Fig. 2c. As shown in Fig. S1,† the WF of V_2O_x films are examined by UPS, and related values of ITO, PEDOT:PSS, PCBM and Ag are also given in previous studies.[52] The WF of V_2O_x (4.74 eV) is lower than that of PEDOT:PSS (5.10 eV),[39] which could lead to the rise in short-circuit current density (J_{SC}), enhancement the

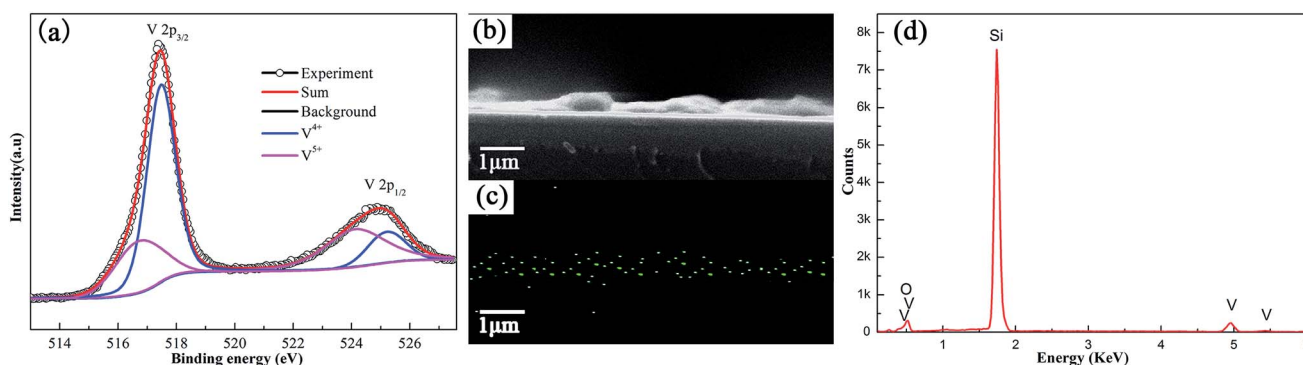**Fig. 1**   (a) The high resolution XPS spectrum corresponding to V in V_2O_x film. The cross-section FESEM image (b), mapping (c) and EDS spectrum (d) for V elemental of V_2O_x film based on monocrystalline silicon.
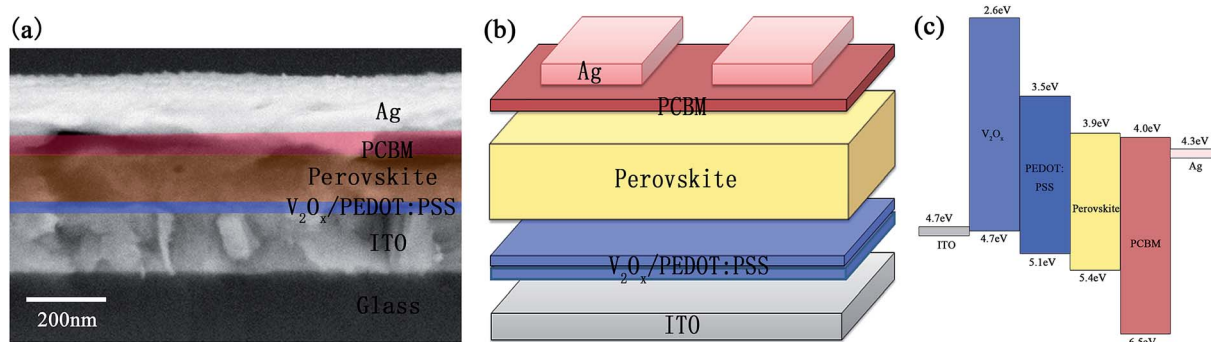
Fig. 2 The cross-section FESEM image (a), the schematic illustration (b) and the energy level diagram (c) of the PSC device with double-decked V_2O_x/PEDOT:PSS film.

extraction of the charge carriers from the absorption layer and reduction the carriers recombination.

In order to analyze the effect of different HTL films on the crystallization of $CH_3NH_3PbI_{3−x}Cl_x$ thin films, we have measured the FESEM images of various HTL films and perovskite thin films based on HTL films. The surface FESEM images of V_2O_x, PEDOT:PSS and V_2O_x/PEDOT:PSS HTL films based on ITO coated glasses are shown in Fig. 3a–c, respectively. It is found that some particles with different sizes (the diameter ranges from 10 nm to 30 mm) are presented on surface of the V_2O_x film. The surfaces of ITO/PEDOT:PSS and ITO/V_2O_x/PEDOT:PSS films are more smooth than that of V_2O_x film, which will be more conducive to the growth of $CH_3NH_3PbI_{3−x}Cl_x$ films. The AFM images of V_2O_x, PEDOT:PSS and V_2O_x/PEDOT:PSS HTL films are shown in Fig. S2a–c.† The surface roughness (root-mean-square, RMS) values of the V_2O_x, PEDOT:PSS and the V_2O_x/PEDOT:PSS HTL films are ~5.7 nm, ~3.3 nm and

~2.5 nm, respectively. Compared with conventional PEDOT:PSS films, the V_2O_x/PEDOT:PSS film has a lower roughness. The roughness of the HTL film has a great influence on the morphology of perovskite films. Fig. 3d–f show surface FESEM images of $CH_3NH_3PbI_{3−x}Cl_x$ thin films based on ITO/V_2O_x, ITO/PEDOT:PSS and ITO/V_2O_x/PEDOT:PSS films respectively. The V_2O_x film with different sizes of particles might be detrimental to the formation of crystal nucleus sites and the growth of crystalline grains, resulting in larger pores (the diameter of pores ranges from 50 nm to 300 mm) on the perovskite film surface based on ITO/V_2O_x. On the contrary, the pores of perovskite film based on ITO/PEDOT:PSS or ITO/V_2O_x/PEDOT:PSS are fewer and smaller, with the diameter of less than 50 nm. Furthermore, compared with the other two perovskite films, the film based on ITO/V_2O_x/PEDOT:PSS shows a larger crystal grains and more uniform surface topography, which results from the smoother V_2O_x/PEDOT:PSS HTL film
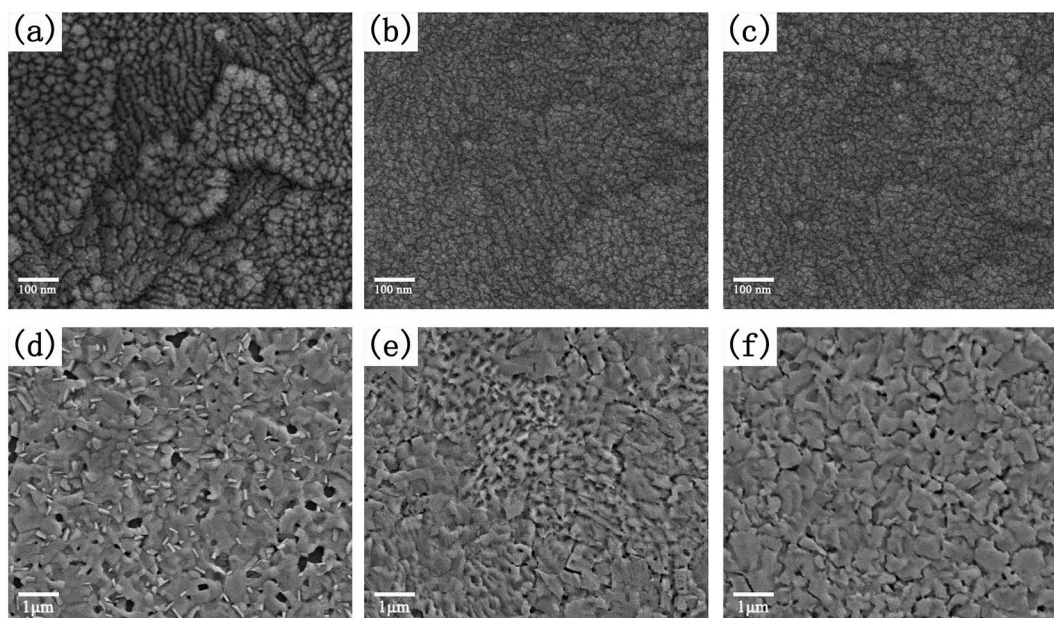

Fig. 3 The surface FESEM images of V_2O_x film (a), PEDOT:PSS film (b) and V_2O_x/PEDOT:PSS HTL film (c) based on ITO coated glasses. The surface FESEM images of $CH_3NH_3PbI_{3−x}Cl_x$ thin films based on ITO/V_2O_x (d), ITO/PEDOT:PSS (e) and ITO/V_2O_x/PEDOT:PSS films (f), respectively.
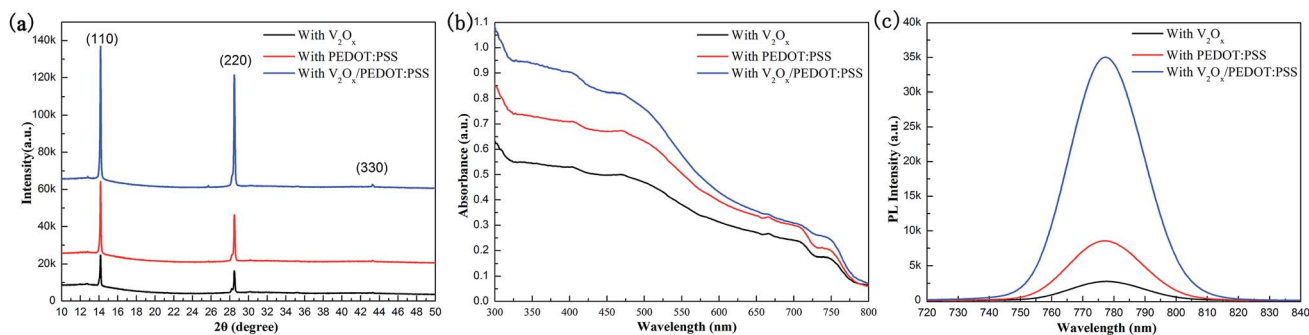
Fig. 4 The XRD spectra (a), the absorbance spectra (b) and the steady-state PL spectra (c) of the $CH_3NH_3PbI_{3-x}Cl_x$ films after being annealed on the V_2O_x film, the pristine PEDOT:PSS film, and the double-decked V_2O_x/PEDOT:PSS composite film, respectively.

(Fig. S2†). This is consistent with the results presented in the XRD pattern (Fig. 4a). The XRD analysis of $CH_3NH_3PbI_{3-x}Cl_x$ films shows diffraction peaks at 14.22°, 28.56°, and 43.29°, corresponding to (110), (220), and (330) planes, respectively. The lattice parameters of $CH_3NH_3PbI_{3-x}Cl_x$ films with tetragonal perovskite structure are $a = 8.825$ Å, $b = 8.835$ Å and $c = 11.24$ Å, similar to that of $CH_3NH_3PbI_3$ previously reported.[10,44] Probably, the weak diffraction peaks of PbI_2 appear at 12.77° and 25.71°, because $CH_3NH_3PbI_{3-x}Cl_x$ film is decomposed into a little PbI_2 under the condition of prolonged annealing. Obviously, compared with other two perovskite films, $CH_3NH_3PbI_{3-x}Cl_x$ thin film with double-decked V_2O_x/PEDOT:PSS film has a better crystallinity, which is in alignment with the FESEM images (Fig. 3d–f). The UV/Vis absorption spectra of the $CH_3NH_3PbI_{3-x}Cl_x$ films spin-coated on the different HTLs are shown in Fig. 4b. The perovskite film with double-decked V_2O_x/PEDOT:PSS layer has a stronger absorption within the ranges of 300–800 nm, compared with other two perovskite films. In order to further confirm performances of the HTLs serving as charge acceptors within the PSCs, steady-state PL measurements were carried out to investigate the quenching of perovskite emission. The quenching of the PL emission by the V_2O_x, PEDOT:PSS and V_2O_x/PEDOT:PSS layers can be clearly observed in Fig. 4c. The steady-state PL response clearly shows that the $CH_3NH_3PbI_{3-x}Cl_x$ films with HTLs appear a PL intensity peak at about 780 nm. It should be noted that the PL intensity of $CH_3NH_3PbI_{3-x}Cl_x$ film with double-decked V_2O_x/PEDOT:PSS layer is the lowest. This indicates that the double-decked V_2O_x/PEDOT:PSS

film plays an important role in quenching recombination channels of electrons and holes in PSC devices.

3.2 The photovoltaic performance of PSCs

In order to compare the properties of different HTL materials, we fabricate three kinds of PSC devices with PEDOT:PSS, V_2O_x/PEDOT:PSS and PEDOT:PSS/V_2O_x HTL films. The photoelectric properties of three PSCs are measured under the illumination of AM 1.5 G simulated solar light at 100 mW cm^{-2}. The J–V curves of the PSC devices are shown in Fig. 5a. In our study, a conventional inverted PHJ PSC device with PEDOT:PSS HTL film is used as reference device. For the device with double-decked PEDOT:PSS/V_2O_x film, although the V_{OC} of it has been improved, its J_{SC} and FF are lowered notably, resulting in its lower PCE. With the bias voltage increase, the current density experiences the process: slight decline—slight increase—rapid decline (Fig. 5a). For this strange phenomenon, we have not found a reasonable explanation. A explanation might be that oxygen deficiencies close to the Fermi level of the material and reduction in doping in the perovskite film,[53,54] result in the increase of current in the process of applying forward bias to PSC device with double-decked PEDOT:PSS/V_2O_x film. Compared with reference device, the performances of PSC device with double-decked V_2O_x/PEDOT:PSS film have been significantly improved, such as the open circuit voltage (V_{OC}), J_{SC}, fill factor (FF) and PCE. The uniform and dense morphology of the perovskite film with

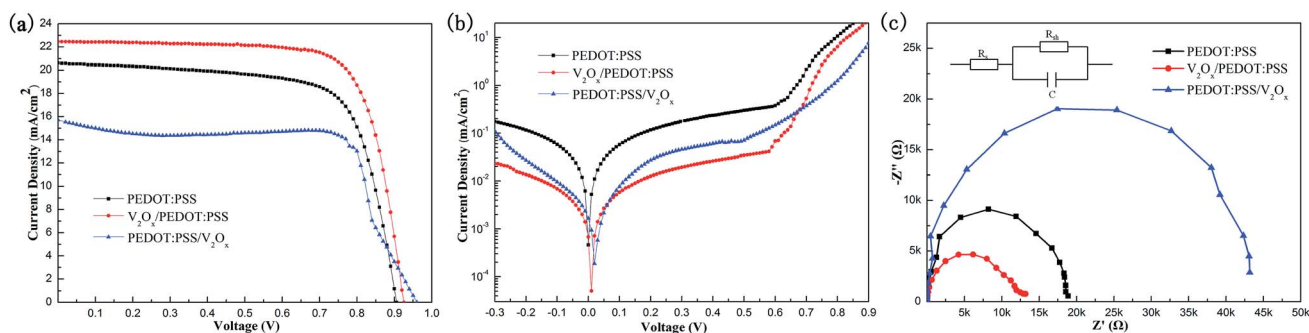**Fig. 5** The J–V curves (a), the dark J–V curves (b) and the EIS spectra with the equivalent circuit (c) of PSCs based on the V_2O_x film, the pristine PEDOT:PSS film, and the double-decked V_2O_x/PEDOT:PSS composite film, respectively.

Table 1 The photovoltaic parameters of the PSC devices with different HTLs

Devices	R_s (Ω)	R_p (kΩ)	C (nF)
With PEDOT:PSS	39.91	18.87	6.25
With V_2O_x/PEDOT:PSS	43.17	13.08	7.36
With PEDOT:PSS/V_2O_x	336.89	43.17	7.61

double-decked V_2O_x/PEDOT:PSS film (Fig. 3f) can effectively avoid defects and achieve a better performance.

To further understand the mechanism of performance improvement of PSCs with the double-decked V_2O_x/PEDOT:PSS HTL, the J–V curves (Fig. 5b) of three devices are recorded in the dark conditions. Dark current measurement is an effective method of evaluating the recombination of free carriers and charge carrier loss in the leakage pathways.[55] It can be shown that the double-decked V_2O_x/PEDOT:PSS and PEDOT:PSS/V_2O_x could simultaneously prevent the leakage current under the condition of reverse bias and improve the current injection under the forward bias. Obviously, the smallest leakage current density and the largest rectification ratio are presented in the dark J–V curve of the device with double-decked V_2O_x/PEDOT:PSS at reverse-biased region, indicating a desired diode characteristics.[56] EIS measurements are performed to analyze the interfacial charge transfer process of devices. The Nyquist plots of three devices with different HTLs are shown in Fig. 5c. The frequency range measured is from 10^6 to 1 Hz with AC amplitude of 10 mV at 0.84 V bias. Each impedance spectra is simulated through an equivalent circuit, forming a semicircle. The photovoltaic parameters of the devices are shown in

Table 1, including series resistance (R_s), parallel resistance (R_p) and capacitance (C). It is found that C is similar among three devices with different HTLs while their R_p are changed regularly. The resistance of charge transport of the device with double-decked V_2O_x/PEDOT:PSS film is the lowest. This indicates that charge transport rate of the device with double-decked V_2O_x/PEDOT:PSS HTL film is the biggest among devices in this study.

The valence state of the vanadium element in the vanadium oxide has exerted a great influence on the conductivity of the HTL thin film and photoelectric properties of the PSC device. In our study, we change the valence of vanadium in the V_2O_x by adjusting the molar ratio (1 : 20, 1 : 40, 1 : 60, 1 : 80 and 1 : 100) of V_2O_5 to H_2O_2. The photograph of various V_2O_x solutions is shown in Fig. 6a. As the proportion of H_2O_2 increases, the color of the V_2O_x solution gradually becomes light. The contents of V^{4+} and V^{4+} of the V_2O_x thin film measured by XPS are shown in Table 2. The content of V^{4+} increases with the ratio of H_2O_2, resulting in a higher conductivity of the double-decked V_2O_x/PEDOT:PSS HTL film. As shown in Fig. 6b–e, the mean and standard deviations of the V_{OC}, J_{SC}, FF and PCE of PSC devices

Table 2 The valence state contents of the V element of V_2O_x thin film with different molar ratios of V_2O_5 to H_2O_2

V element	Molar ratios of V_2O_5 to H_2O_2				
	1 : 20	1 : 40	1 : 60	1 : 80	1 : 100
V^{4+}	33.52%	38.13%	41.47%	43.97%	45.38%
V^{5+}	66.48%	61.87%	58.53%	56.03%	54.62%
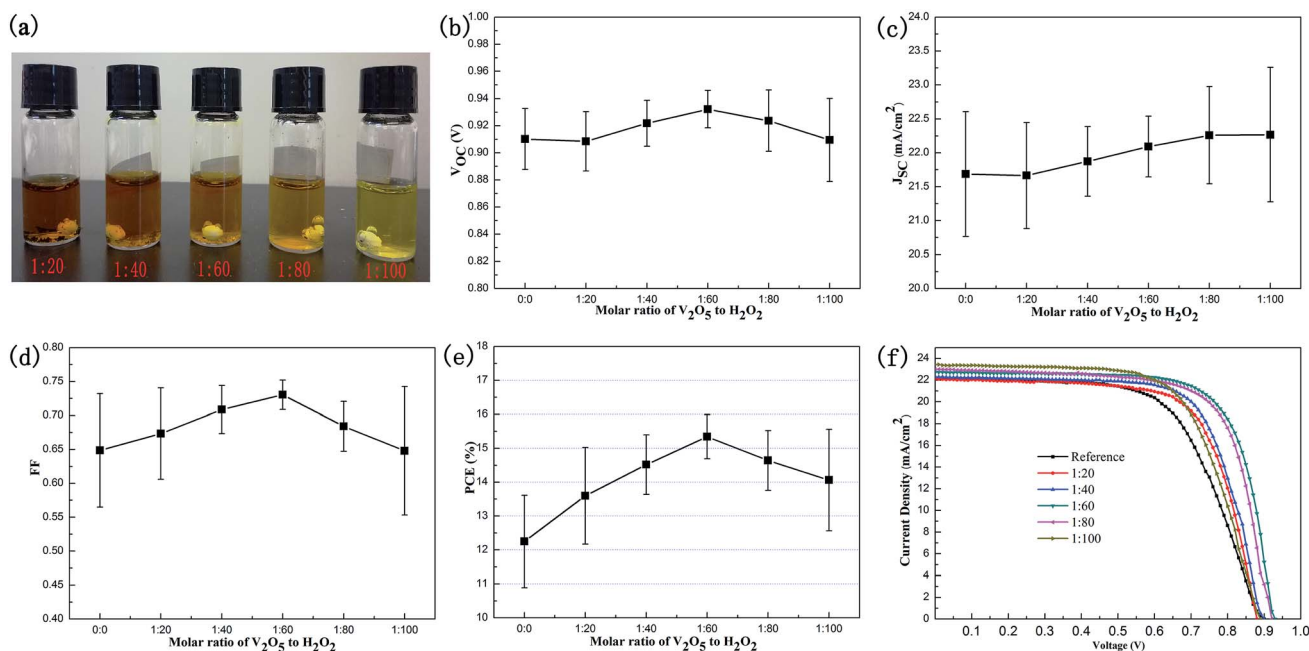
Fig. 6 (a) The photograph of the V_2O_x solution prepared by mixing V_2O_5 and H_2O_2 at different molar ratios (1 : 20, 1 : 40, 1 : 60, 1 : 80 and 1 : 100). The mean and standard deviations of the V_{OC} (b), J_{SC} (c), FF (d) and PCE (e), and the J–V curves (f) of the PSC devices with double-decked V_2O_x/PEDOT:PSS HTL film with different molar ratios of H_2O_2 to V_2O_5.
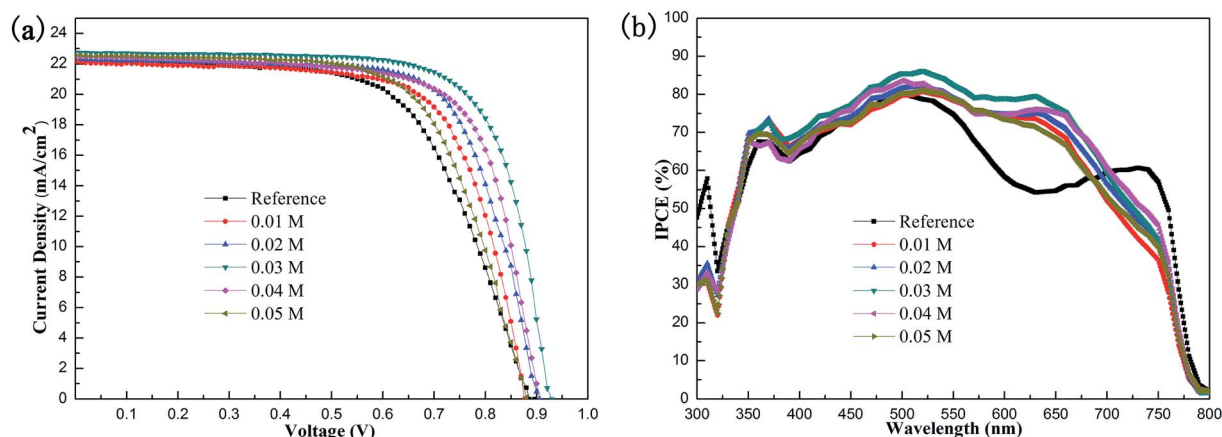
Fig. 7 The J–V curves (a) and IPCE spectra (b) of PSC based on pristine PEDOT:PSS and double-decked V_2O_x/PEDOT:PSS HTL film with varied-concentration V_2O_x solution (0.01, 0.02, 0.03, 0.04 and 0.05 M).

with different molar ratios of H_2O_2 to V_2O_5 are calculated. It is found that the J_{SC} increases with molar ratio of H_2O_2 to V_2O_5. The conductivity of the double-decked V_2O_x/PEDOT:PSS HTL film improves with the increase of V^{4+}, thus the J_{SC} of the device increases. However, the V_{OC}, FF and PCE show a trend—increase and then decline. Possibly, the decline of V^{5+} results in less doping and more defects of V_2O_x thin film, as well as a lower performance of device. The best-performance (Fig. 6f) and high-reproducibility device is achieved when the molar ratio of V_2O_5 to H_2O_2 is 1 : 60, namely, the content of V^{4+} is 41.5%.

The concentration of V_2O_x solution has a great influence on the thickness and uniformity of the double-decked V_2O_x/PEDOT:PSS HTL film. Therefore, we prepare V_2O_x solutions with different concentration gradients (0.01, 0.02, 0.03, 0.04 and 0.05 M). The J–V characteristics of PSC based on pristine PEDOT:PSS and double-decked V_2O_x/PEDOT:PSS HTL film with varied concentration of V_2O_x solution are shown in Fig. 7a. The Table 3 shows the key performance parameters of PSCs, including V_{OC}, J_{SC}, FF and PCE. The best performance of device is achieved under the concentration of 0.03 M of V_2O_x solutions. With the increase of concentration of the V_2O_x solution, all performance parameters of devices show a trend, that is, increase first and then decrease, except J_{SC}. The reason why J_{SC} keeps rising is that a higher concentration of V_2O_x solution allows the V_2O_x film to have a larger contact area with the PEDOT:PSS film. The thickness of the double-decked V_2O_x/PEDOT:PSS HTL film increases with concentration of V_2O_x

solution. On the one hand, when the concentration of V_2O_x solution is very low, the V_2O_x particles excessively disperse, failing to form the film. On the other hand, when the concentration of V_2O_x solution gets very high, the film has a higher roughness. Moreover, there is a large barrier to extraction through the metal oxide valence band, because the V_2O_x/PEDOT:PSS layer is too thick to allow the tunnelling of charges. There is no doubt that these two aspects of the factors are not conducive to preparing high-performance devices. Fig. 7b shows the IPCE spectra of the PSCs based on pristine PEDOT:PSS and double-decked V_2O_x/PEDOT:PSS HTL film. Compared with the conventional AM 1.5 solar radiation spectrum,[57] interestingly, the IPCE of devices based on V_2O_x/PEDOT:PSS increases within a wide wavelength range between 500 and 700 nm, indicating that the devices with double-decked V_2O_x/PEDOT:PSS HTL can absorb more solar energy and convert it into electrical energy. In particular, the performance of the device with 0.03 M V_2O_x is the best among devices.

The best performance of PSC device is achieved by controlling the optimal molar ratio of V_2O_5 to H_2O_2 and the concentration of the V_2O_x solution. The J–V curve and main parameters (V_{OC}, J_{SC}, FF and PCE) of the best-performance device with the double-decked V_2O_x/PEDOT:PSS HTL film are shown in Fig. 8a. A best PCE of 15.86%, corresponding to a J_{SC} of 22.69 mA cm^{-2}, a V_{OC} of 0.93 V, and a FF of 0.75, is achieved. In our study, as shown in the histograms of PCE parameters of reference devices with PEDOT:PSS HTL (30 cells) (inset) and controllable devices with the double-decked V_2O_x/PEDOT:PSS HTL (120 cells)

Table 3 The main performance parameters of PSCs with varied concentration of V_2O_x solution

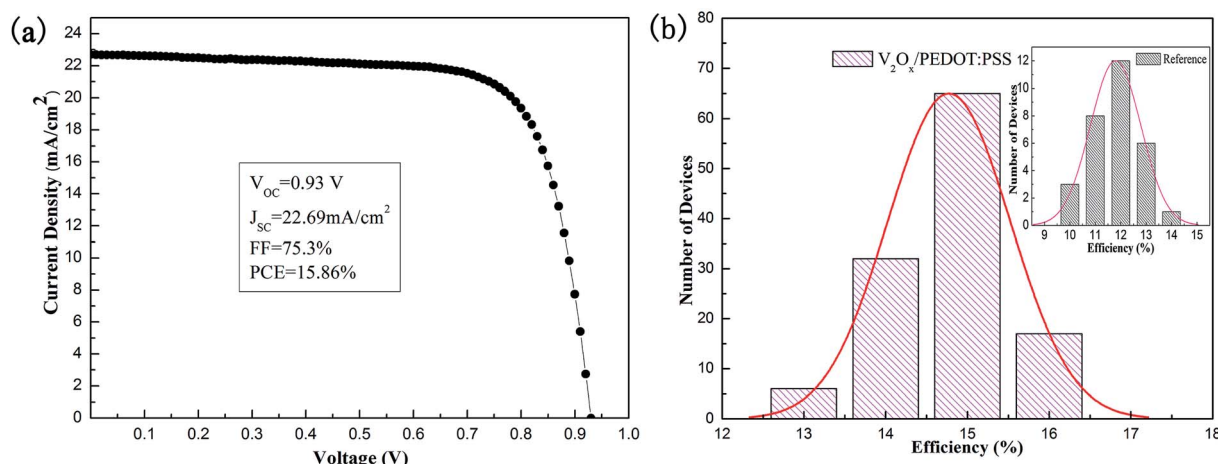| Devices	V_{OC} (V)	J_{SC} (mA cm^{-2})	FF	PCE (%)
Reference	0.92(0.91 ± 0.03)	22.25(21.26 ± 1.07)	0.72(0.67 ± 0.07)	13.56(11.85 ± 1.81)
0.01 M	0.93(0.92 ± 0.02)	22.15(21.23 ± 0.98)	0.72(0.68 ± 0.06)	14.95(13.53 ± 1.75)
0.02 M	0.94(0.93 ± 0.02)	22.19(21.57 ± 0.75)	0.73(0.71 ± 0.03)	15.32(14.17 ± 1.17)
0.03 M	0.94(0.93 ± 0.01)	22.41(21.96 ± 0.51)	0.75(0.74 ± 0.02)	15.86(14.97 ± 0.91)
0.04 M	0.93(0.92 ± 0.01)	22.63(21.97 ± 0.89)	0.74(0.73 ± 0.03)	15.67(14.75 ± 0.99)
0.05 M	0.93(0.91 ± 0.04)	23.12(21.99 ± 1.19)	0.74(0.66 ± 0.09)	15.18(13.98 ± 1.69)

Fig. 8 (a) The J–V curve and main parameters of the best-performance device with the double-decked V_2O_x/PEDOT:PSS HTL film. (b) The histogram of PCEs of 120 double-decked V_2O_x/PEDOT:PSS HTL controlled devices. Inset is the histogram of PCEs of 30 reference devices with PEDOT:PSS HTL. (Gaussian distributions were fit to obtain the average and relative standard deviations.)

(Fig. 8b), the devices performance follows a Gaussian distribution and achieves the PCE_{AVE} of 11.85% and 14.97% respectively. The relative standard deviations of the reference devices and devices based on the V_2O_x/PEDOT:PSS are 9.8% and 4.5%, respectively, indicating that the latter shows a better reproducibility than the former.

4. Conclusions

With hard efforts we have successfully used solution-processed double-decked V_2O_x/PEDOT:PSS film as HTL of high-performance inverted planar PSCs. In our study, the best performance of the devices has been achieved by changing the valence of vanadium of double-decked V_2O_x/PEDOT:PSS film. Furthermore, the device performance has been optimized by controlling the optimum concentration of the V_2O_x solution. The results show that the double-decked V_2O_x/PEDOT:PSS film plays an essential role in improving charge transfer rate and suppressing the electron–hole pair recombination. With this double-decked film, the PCE and reproducibility of PSCs have been improved significantly.

Acknowledgements

Notes and references

1 M. Grätzel, *Nat. Mater.*, 2014, **13**, 838–842.

2 N. G. Park and J. Phys, *Chem. Lett.*, 2013, **4**, 2423–2429.

3 T. Baikie, Y. Fang, J. M. Kadro, M. Schreyer, F. X. Wei, S. G. Mhaisalkar, M. Graetzel and T. J. White, *J. Mater. Chem. A*, 2013, **1**, 5628–5641.

4 G. C. Xing, N. Mathews, S. Y. Sun, S. S. Lim, Y. M. Lam, M. Grätzel, S. Mhaisalkar and T. C. Sum, *Science*, 2013, **342**, 344–347.

5 S. D. Stranks, G. E. Eperon, G. Grancini, C. Menelaou, M. J. P. Alcocer, T. Leijtens, L. M. Herz, A. Petrozza and H. J. Snaith, *Science*, 2013, **342**, 341–344.

6 W. Nie, H. Tsai, R. Asadpour, J. C. Blancon, A. J. Neukirch, G. Gupta, J. J. Crochet, M. Chhowalla, S. Tretiak and M. A. Alam, *Science*, 2015, **347**, 522–525.

7 G. E. Eperon, V. M. Burlakov, P. Docampo, A. Goriely and H. J. Snaith, *Adv. Funct. Mater.*, 2014, **24**, 151–157.

8 B. Conings, L. Baeten, C. D. Dobbelaere, J. D'Haen, J. Manca and H. G. Boyen, *Adv. Mater.*, 2014, **26**, 2041–2046.

9 C. G. Wu, C. H. Chiang, Z. L. Tseng, M. K. Nazeeruddin, A. Hagfeldt and M. Grätzel, *Energy Environ. Sci.*, 2015, **8**, 2725–2733.

10 A. Kojima, K. Teshima, Y. Shirai and T. Miyasaka, *J. Am. Chem. Soc.*, 2009, **131**, 6050–6051.

11 NREL, http://www.nrel.gov/ncpv/images/efficiency_chart.jpg, accessed 10 April 2016.

12 W. Ke, D. Zhao, C. R. Grice, A. J. Cimaroli, J. Ge, H. Tao, H. Lei, G. Fang and Y. Yan, *J. Mater. Chem. A*, 2015, **3**, 17971–17976.

13 M. Qian, M. Li, X. Shi, H. Ma, Z. K. Wang and L. Liao, *J. Mater. Chem. A*, 2015, **3**, 13533–13539.

14 Q. Chen, H. Zhou, Z. Hong, S. Luo, H. S. Duan, H. H. Wang, Y. Liu, G. Li and Y. Yang, *J. Am. Chem. Soc.*, 2013, **136**, 622–625.

15 D. Liu and T. L. Kelly, *Nat. Photonics*, 2014, **8**, 133–138.

16 H. S. Kim, C. R. Lee, J. H. Im, K. B. Lee, T. Moehl, A. Marchioro, S. J. Moon, R. Humphry-Baker, J. H. Yum, J. E. Moser, M. Grätzel and N. G. Park, *Sci. Rep.*, 2012, **2**, 591–597.

17 F. Zuo, S. T. Williams, P. W. Liang, C. C. Chueh, C. Y. Liao and A. K. Y. Jen, *Adv. Mater.*, 2014, **26**, 6454–6460.

18 M. A. Green, A. Ho-Baillie and H. J. Snaith, *Nat. Photonics*, 2014, **8**, 506–514.

19 Y. C. Shao, Z. G. Xiao, C. Bi, Y. B. Yuan and J. S. Huang, *Nat. Commun.*, 2014, **5**, 5784–5790.

20 C. Zuo and L. Ding, *Nanoscale*, 2014, **6**, 9935–9938.

21 Z. Xiao, Q. Dong, C. Bi, Y. Shao, Y. Yuan and J. Huang, *Adv. Mater.*, 2014, **26**, 6503–6509.

22 J. Seo, S. Park, Y. C. Kim, N. J. Jeon, J. H. Noh, S. C. Yoon and S. I. Seok, *Energy Environ. Sci.*, 2014, **7**, 2642–2646.

23 S. W. Tong, C. F. Zhang, C. Y. Jiang, G. Liu, Q. D. Ling, E. T. Kang, D. S. H. Chan and C. X. Zhu, *Chem. Phys. Lett.*, 2008, **453**, 73–76.

24 S. Jönsson, J. Birgerson, X. Crispin, G. Greczynski, W. Osikowicz, A. W. Denier van der Gon, W. R. Salaneck and M. Fahlman, *Synth. Met.*, 2013, **139**, 1–10.

25 Y. H. Kim, C. Sachse, M. L. Machala, C. May, L. Müller-Meskamp and K. Leo, *Adv. Funct. Mater.*, 2011, **21**, 1076–1081.

26 J. H. Kim, P. W. Liang, S. T. Williams, N. Cho, C. C. Chueh, M. S. Glaz, D. S. Ginger and A. K. Y. Ken, *Adv. Mater.*, 2015, **27**, 695–701.

27 J. Y. Jeng, K. C. Chenk, T. Y. Chiang, P. Y. Lin, T. D. Tsai, Y. C. Chang, T. F. Guo, P. Chen, T. C. Wen and Y. J. Hsu, *Adv. Mater.*, 2014, **26**, 4107–4113.

28 J. Cui, F. Meng, H. Zhang, K. Cao, H. Yuan, Y. Cheng, F. Huang and M. Wang, *ACS Appl. Mater. Interfaces*, 2014, **6**, 22862–22870.

29 Z. Zhu, Y. Bai, T. Zhang, Z. Liu, X. Long, Z. Wei, Z. Wang, L. Zhang, J. Wang, F. Yan and S. Yang, *Angew. Chem., Int. Ed.*, 2014, **53**, 12571–12783.

30 L. Hu, W. Wang, H. Liu, J. Peng, H. Cao, G. Shao, Z. Xie, W. Ma and J. Tang, *J. Mater. Chem. A*, 2015, **3**, 515–518.

31 V. Shrotriya, G. Li, Y. Yao, C. W. Chu and Y. Yang, *Appl. Phys. Lett.*, 2006, **88**, 73508–73510.

32 I. Hancox, K. V. Chauhan, P. Sullivan, R. A. Hatton, A. Moshar, C. P. A. Mulcahy and T. S. Jones, *Energy Environ. Sci.*, 2010, **3**, 107–110.

33 D. Y. Kim, J. Subbiah, G. Sarasqueta, F. So, H. Ding, Irfan and Y. Gao, *Appl. Phys. Lett.*, 2009, **95**, 93304–93308.

34 A. K. K. Kyaw, X. W. Sun, C. Y. Jiang, G. Q. Lo, D. W. Zhao and D. L. Kwong, *Appl. Phys. Lett.*, 2008, **93**, 221107–221109.

35 F. C. Krebs, *Sol. Energy Mater. Sol. Cells*, 2009, **93**, 465–475.

36 O. Hagemann, M. Bjerring, N. C. Nielsen and F. C. Krebs, *Sol. Energy Mater. Sol. Cells*, 2008, **92**, 1327–1335.

37 D. Y. Lee, S. I. Na and S. S. Kim, *Nanoscale*, 2016, **8**, 1513–1522.

38 F. Hou, Z. Su, F. Jin, X. Yan, L. Wang, H. Zhao, J. Zhu, B. Chu and W. Li, *Nanoscale*, 2015, **7**, 9427–9432.

39 H. Peng, W. Sun, Y. Li, S. Ye, H. Rao, W. Yan, H. Zhou, Z. Bian and C. Huang, *Nano Res.*, 2016, **9**, 2960–2971.

40 J. Liu, Q. Li, T. Wang, D. Yu and Y. Li, *Angew. Chem.*, 2004, **116**, 5158–5162.

41 H. Phetmung, T. W. Kim, S. J. Hwang and J. H. Choy, *J. Iran. Chem. Soc.*, 2008, **5**, 706–711.

42 X. Wu, Y. Tao, L. Dong and J. Hong, *J. Mater. Chem.*, 2004, **14**, 901–904.

43 Y. Liu, M. Bag, L. A. Renna, Z. A. Page, P. Kim, T. Emrick, D. Venkataraman and T. P. Russell, *Adv. Energy Mater.*, 2016, **6**, 1501606–1501612.

44 M. M. Lee, J. Teuscher, T. Miyasaka, T. N. Murakami and H. J. Snaith, *Science*, 2012, **338**, 643–647.

45 Z. Liu, T. He, H. Wang, X. Song, H. Liu, J. Yang, K. Liu and H. Ma, *RSC Adv.*, 2017, **7**, 18456–18465.

46 M. Saliba, T. K. Wee, S. Hiroaki, D. T. Moore, S. Trent, W. Zhang, L. A. Estroff, W. Ulrich and H. J. Snaith, *J. Phys. Chem. C*, 2014, **118**, 17171–17177.

47 H. L. Hsu, C. P. Chen, J. Y. Chang, Y. Y. Yu and Y. K. Shen, *Nanoscale*, 2014, **6**, 10281–10288.

48 S. Bai, Z. W. Wu, X. J. Wu, Y. Z. Jin, N. Zhao, Z. H. Chen, Q. Q. Mei, X. Wang, Z. Z. Ye and T. Song, *Nano Res.*, 2014, **12**, 1749–1758.

49 M. Schindler, F. C. Hawthorne and W. H. Baur, *Chem. Mater.*, 2000, **12**, 1248–1259.

50 L. Pettersson, I. Andersson and A. Gorzsás, *Coord. Chem. Rev.*, 2003, **237**, 77–87.

51 D. Manno, A. Serra, M. Di Giulio, G. Micocci, A. Taurino, A. Tepore and D. Berti, *J. Appl. Phys.*, 1997, **81**, 2709–2714.

52 J. Y. Jeng, Y. F. Chiang, M. H. Lee, S. R. Peng, T. F. Guo, P. Chen and T. C. Wen, *Adv. Mater.*, 2013, **25**, 3727–3732.

53 K. Kanai, K. Koizumi, S. Ouchi, Y. Tsukamoto, K. Sakanoue, Y. Ouchi and K. Seki, *Org. Electron.*, 2010, **11**, 188–194.

54 M. Vasilopoulou, L. C. Palilis, D. G. Georgiadou, A. M. Douvas, P. Argitis, S. Kennou, L. Sygellou, G. Papadimitropoulos, I. Kostis, N. A. Stathopoulos and D. Davazoglou, *Adv. Funct. Mater.*, 2011, **21**, 1489–1497.

55 K. Sun, J. Chang, F. H. Isikgor, P. Li and J. Ouyang, *Nanoscale*, 2015, **7**, 896–900.

56 C. He, C. Zhong, H. Wu, R. Yang, W. Yang, F. Huang, G. C. Bazan and Y. Cao, *J. Mater. Chem.*, 2010, **20**, 2617–2622.

57 GB/T 17683.1-1999, Solar energy-reference solar spectral irradiance at the ground at different receiving conditions-part 1: direct normal and hemispherical solar irradiance for air mass 1.5.